REYNOLDS AND NORMAL STRESSES OF TURBULENT BOUNDARY LAYERS AND CHANNEL/PIPE FLOWS AT MODERATE KÁRMÁN NUMBERS

Matthias H. Buschmann
Institut für Luft – und Kältetechnik Dresden
Bertolt-Brecht Allee 20, 01309 Dresden, GERMANY
Matthias.Buschmann@ilkdresden.de

Mohamed Gad-el-Hak
Department of Mechanical Engineering
Virginia Commonwealth University, Richmond, Virginia, USA
gadelhak@vcu.edu

ABSTRACT

It has been known for a few decades that pure inner scaling does not collapse the characteristic parameters of streamwise stress such as peak value and peak position. Herein we show that this is also true for the Reynolds shear stress and the two other normal stresses. Even more, an analysis of the wall values of streamwise skewness and flatness indicates Kármán number dependencies of these parameters. Employing the alternative mixed scaling, which is based on $u_\tau^{2-\alpha}u_e^{\alpha}$ instead on u_τ^2, these dependencies are removed. Based on the general finding that both inner and outer scales are relevant throughout the entire wall layer, a model for the fluctuations is proposed. From this model all stresses and higher-order moments can be built up.

INTRODUCTION

Are there differences between confined and semi-confined canonical turbulent flows? Between boundary layers on flat plates (ZPG TBL) and flows in straight channels (CHF) or circular pipes (PF)? And if so, what are those differences? Is it just that some parameters such as peak positions and values of Reynolds and normal stresses are different, or are there different physical mechanism underlying the dissimilarities? To answer these questions is most important for understanding wall-bounded flows in general, to find proper scaling laws, and to find correct model assumptions that can be applied, e.g. in numerical simulations.

The questions raised above—but not the answers—have been known for over a decade (Nieuwstadt & Bradshaw, 1997), but have attained intensified interest very recently (Buschmann & Gad-el-Hak, 2010; Jimenez et al., 2010; Marusic et al., 2010). Herein we extend our previous work on the subject. Specifically, we are looking for all peak values and positions of the stresses of ZPG TBL, and CHF and PF at moderate Kármán numbers. For that purpose we have compiled an extensive database[1] of DNS and experimental results.

[1] For details and the symbol colors employed in Fig. 1, see Buschmann & Gad-el-Hak (2010).

Simple analysis reveals the differences of the flow types under consideration. Without claim of completeness, the two most distinct disparities are:

- While confined flows are parallel in the mean, the streamlines of ZPG TBL are divergent.
- Turbulent boundary layers do not experience the influence of an opposite wall, and conversely CHF and PF do not have a free stream.

However, there might even be differences between CHF and PF. While in CHF, the space for turbulence to be transported and to develop is constant along the wall-normal coordinate, that space is successively reduced to zero toward the centerline in PF. This may lead to more and intense interactions between turbulent structures in the latter case.

CLASSICAL INNER SCALING

Figure 1 shows peak positions (left) and peak values (right) of Reynolds and normal stresses versus Kármán number ($\delta^+ = \delta\ u_\tau/\nu$). Due to the minute differences to be expected we have used only DNS results for precision. However, the results that are reported herein are mainly confirmed by carefully selected experimental data. Some of the plots clearly show two branches, one for ZPG TBL (semi-confined flow) and one for CHF and PF (both confined flow). The separate CHF/PF-branches are nowhere split into two sub-branches, which would indicate less significant differences between CHF and PF. The identified differences are marked with rose arrows or bands. While the arrows indicate a growing departure between the two branches, the bands indicate a more or less constant difference, independent of the Kármán number. Linear-linear, semi-logarithmic and log-log plots were tested. In case that one of the plot types leads to linearly-ordered data, this special plot was chosen for Fig. 1, otherwise semi-log plots were selected. This strategy confirmed that the peak positions of the Reynolds shear stress (Fig. 1a) and the streamwise stress (Fig. 1d) have a power-law dependency on the Kármán number.

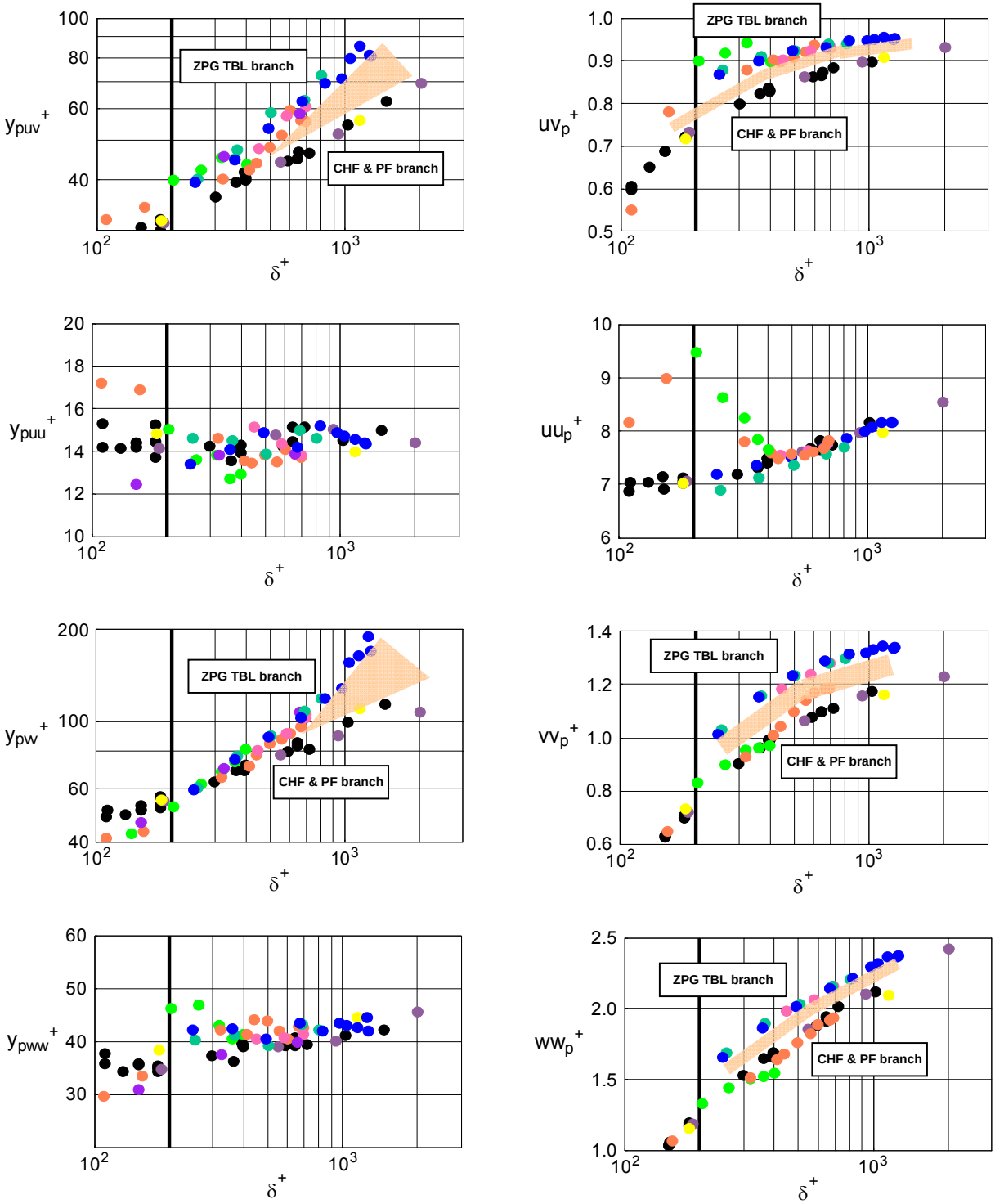

Figure 1: Peak positions (left) and peak values (right) of turbulent stresses. From top to bottom: Reynolds shear-stress, streamwise stress, wall-normal stress, and cross-flow stress. Rose arrows and band indicate regions with increasing differences between ZPG TBL and CHF & PF. Those arrows and bands indicate differences between confined and semi-confined flows. Black bold-line marks lower border of fully-developed turbulent flow at δ^+=200.

The differences in the stresses should be more visible in the *v'*-fluctuations because of their strong connection with wall-normal variation of the mean static pressure. And indeed an increasing difference of the peak position of the wall-normal stress is found in Fig. 1. Interestingly enough the peak position of normal-stress is found to be in close local coincidence with the outer edge of the logarithmic region of the mean-velocity profile. The difference between the *vv*-peak values is nearly Kármán number independent in the analyzed δ^+-range (Fig. 1f). The same is true for peak position and value of the Reynolds stress (Figs. 1a, b). The only stress that does not show any differences in either the peak position or peak value is the streamwise stress. This finding is in agreement with the results of many groups. The *uu*-peak position is located at y^+-value of about 14–15 for all geometries. The *uu*-peak value increases linearly with Kármán number. For low δ^+-values, however, transitional ZPG TBL's have to develop to this common curve. Obviously, the initiation of the flow defines how this takes place (see Fig. 6 in Marusic et al., 2010). There is no observed difference between the peak positions of the cross-flow stress. However, there is a nearly constant displacement between the peak values of ZPG TBL and CHF/PF of the *ww*-stress. That is especially surprising because *u'*- and *w'*-fluctuations have the same degree of freedom and they are not blocked by the wall as the *v'*-fluctuation.

In parting, our results show that there are distinct differences between zero-pressure-gradient turbulent boundary layers and channel/pipe flows. This is in close agreement with the conclusions of Mathis et al. (2009) and Monty et al. (2009).

ALTERNATIVE MIXED SCALING

The observed dependency of the stresses on the Kármán number can be removed to a large extent when shifting to mixed scaling. This scaling is based on $u_\tau^{2-\alpha} u_e^{\alpha}$, instead of on u_τ^2. Here, u_τ denotes the friction velocity, and u_e is the velocity at the outer edge of the boundary layer or at the centerline of a channel/pipe flow. Several attempts have been made to determine an optimum exponent α. The best known was presented by DeGraaff & Eaton (2000), who set α equal to unity. In general, no physical or mathematical arguments exist so far to derive α directly from first principles. Therefore, the value of α is empirically determined. Buschmann et al. (2009) found from an extensive analysis of DNS and experimental results an α-value of ½. This value applies successfully to the peak values of stresses especially in the streamwise direction. To distinguish the scaling based on α = ½ from the mixed scaling based on α = 1 by DeGraaff & Eaton (2000), Buschmann et al. (2009) named their approach *alternative mixed scaling*.

One of the objectives of the present study is to show that there is a possibility to scale skewness and flatness in such a way as to remove the Kármán number dependencies. Figures 2a and 2c show the wall values of skewness and flatness of the streamwise fluctuations from several DNS realizations and experiments. A non-monotonically Kármán number dependency is clearly discernible. Below δ^+=200, both parameters decrease with increasing Kármán number. Above this threshold an increase is observed. While the flow in the first region may be dominated by low-Reynolds-number effects, an influence of outer scales that persists for very high Reynolds numbers has to be considered in the second region.

Once again the idea of alternative mixed scaling is employed. In general, the following *correction* of inner-scaled skewness and flatness of the streamwise fluctuations has to be applied:

$$S_u^{\#} = S_u^{+} \left(\frac{u_\tau}{u_e}\right)^{1/2} \qquad F_u^{\#} = F_u^{+} \left(\frac{u_\tau}{u_e}\right) \qquad (1)$$

Here, the superscript + denotes classical inner scaling and # alternative mixed scaling according to Buschmann et al. (2008). Details of the applied scaling are given in Table 1. The moments for the two remaining fluctuation components and the mixed moments can be derived in a similar manner.

The achieved improvements with respect to the wall values of skewness and flatness are illustrated in Figures 2b and 2d, as well as Table 2. The plots reveal that the low-Reynolds-number effects (below $\delta^+ = 200$) are not removed. However, above this value the wall values of skewness and flatness show nearly constant values of about, respectively, $S_{uw}^{\#}$ = 0.216 and $F_{uw}^{\#}$ = 0.216. The percentage differences between first and last wall values of skewness and flatness employing classical and alternative mixed scaling are compiled in Table 2. The improvement when applying alternative mixed scaling is remarkable. That seems to be for both confined as well as for semi-confined flows. However, one has to note the quite different Kármán number ranges in the different data sets, which makes it difficult to compare them directly.

MODEL OF FLUCTUTION

The foregoing results led us to the following three hypotheses:

- Any model for the stresses and higher-order moments should reflect both inner and outer scales.
- Any scaling must start from the fluctuations directly.
- Mean profiles and the time-averaged moments of the fluctuations have to be built up from these fluctuations.

With our fourth argument we go back to the classical integral parameters (displacement thickness, momentum and energy lost thickness, etc.). Only the entirety of these parameters contains the same amount of information as the mean velocity profile itself. Analogously we argue that only the entirety of all time-averaged statistical moments contains the same amount of information as the fluctuations themselves. The consequence is that any validation of a fluctuation model has to consider more than just the stresses. Higher-order moments should be represented in an equivalent quality as the second order moments.

Table 1: Scaling of second to fourth moments of streamwise fluctuations.

n	n^{th}-moment classical inner scaling	n^{th}-moment alternative mixed scaling
2	$\langle u'^2\rangle^+ = \frac{\langle u'^2\rangle}{u_\tau^2}$	$\langle u'^2\rangle^\# = \frac{\langle u'^2\rangle}{u_\tau^{6/4}u_e^{2/4}}$
3	$\langle u'^3\rangle^+ = \frac{\langle u'^3\rangle}{u_\tau^3}$	$\langle u'^2\rangle^\# = \frac{\langle u'^3\rangle}{u_\tau^{7/4}u_e^{5/4}}$
4	$\langle u'^4\rangle^+ = \frac{\langle u'^4\rangle}{u_\tau^4}$	$\langle u'^2\rangle^\# = \frac{\langle u'^4\rangle}{u_\tau^{8/4}u_e^{8/4}}$

Table 2: Percentage difference between first and last value of skewness and flatness employing different scaling approaches (only values above δ^+=200 are considered).

Authors	δ^+-range	$S_{uw}{}^+$	$S_{uw}{}^\#$	$F_{uw}{}^+$	$F_{uw}{}^+$
Schlatter ZPG TBL DNS	252-1271	-17.8	-4.6	-22.1	3.7
Simens et al. ZPG TBL DNS	445-690	-5.6	-1.0	no data	no data
Hu et al. CHF DNS	361-1451	-11.6	-1.8	-14.3	4.6
Nagano et al. Exp. TBL	407-656	9.2	6.9	8.3	3.6
Fernholz et al. Exp. TBL	930-1694	2.0	-1.4	7.4	0.8

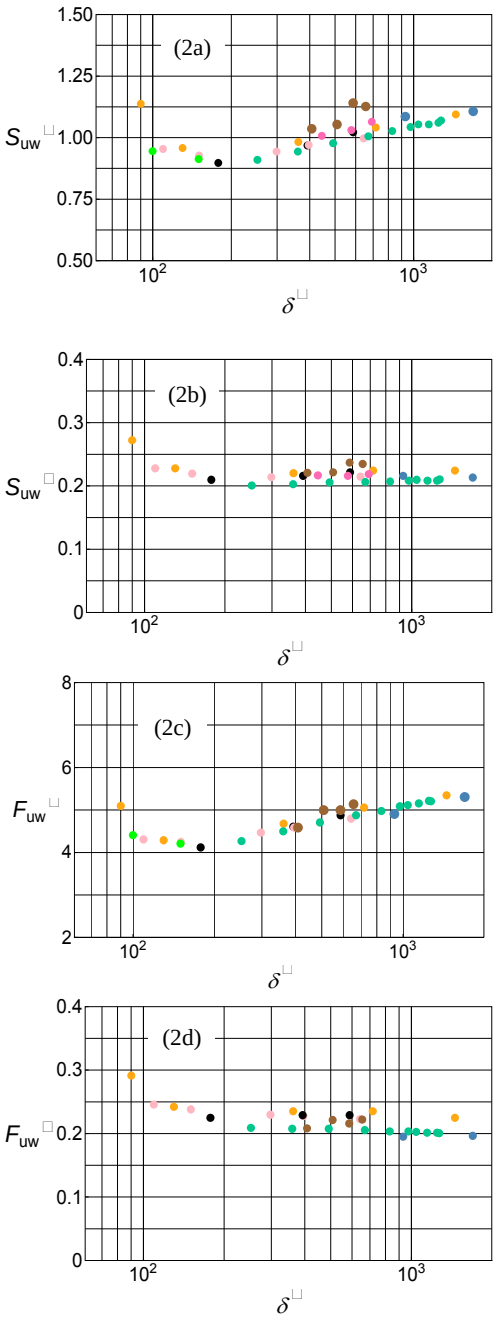

Figure 2: Wall values of skewness and flatness of several DNS and experimental results. From top: skewness classical inner scaling; skewness alternative mixed scaling; flatness classical scaling; and flatness alternative mixed scaling.
• Jimenéz et al. (2010) ZPG TBL DNS; • Schlatter et al. (2009) ZPG TBL DNS; • Hu et al. (2006) CH DNS; • Kim et al. (1987) CH DNS ; • Iwamoto et al. (2002) CH DNS; • Nagano et al. (1992) exp. ZPG TBL; • Bruns et al. (1992) exp. ZPG TBL

To derive a model[2] according to these three hypotheses we start with Reynolds decomposition:

$$u^+ = \langle u^+ \rangle + u'^+ \qquad (2)$$

where u^+ denotes the velocity in the streamwise direction. Squared brackets denote time averaging and apostrophe the instantaneous part. Our goal is to conduct an asymptotic matching of inner eq. (3) and outer expansions eq. (4) to get an expression for u^+.

$$u^+ = \frac{1}{\kappa} \ln y^+ + \sum_{j=0}^{n} A_{i,j} \frac{1}{y^{+j}} \qquad (3)$$

$$U = 1 + \varepsilon \left[\frac{1}{\kappa} \ln \eta + \sum_{j=0}^{m} A_{o,j} \eta^j \right] \qquad (4)$$

Here, the subscript i stands for inner and o for outer region. The coefficients $A_{i,j}$ and $A_{o,j}$ are supposed to be random functions of space and time. By asymptotic matching of (3) and (4) and time averaging the mean velocity, (5) is obtained. The streamwise fluctuation (6) follows by definition from eq. (2) by subtracting the mean profile from u^+.

$$\langle u^+ \rangle = \frac{1}{\kappa} \ln y^+ + \sum_{j=0}^{n} \langle A_{i,j} \rangle \frac{1}{y^{+j}} + \sum_{j=1}^{m} \langle A_{o,j} \rangle \eta^j \qquad (5)$$

$$u'^+ = \sum_{j=0}^{m} A'_{i,j} \frac{1}{y^{+j}} + \sum_{j=1}^{m} A'_{o,j} \eta^j \qquad (6)$$

For the final prediction of stresses and higher-order moments, it is argued that inner and outer time scales are different. Therefore, the coefficients of eq. (6) are decomposed in products of time-independent ($a_{i,j}$, $a_{o,j}$) and time-dependent (A'_i, A'_o) factors:

$$A'_{i,j} = a_{i,j} A'_i \qquad A'_{o,j} = a_{o,j} A'_o \qquad (7)$$

For simplification the time-independent parts of the first term of (6) are substituted by D_u, and of the second term by E_u. The streamwise stress, the third moment and all higher moments then follow from their respective definitions.

$$\langle u'^2 \rangle^+ = \langle A'^2_i \rangle D_u^2 + 2 \langle A'_i A'_o \rangle D_u E_u + \langle A'^2_o \rangle E_u \qquad (8)$$

$$\langle u'^3 \rangle^+ = \langle A'^3_i \rangle D_u^3 + 3 \langle A'^2_i A'_o \rangle D_u^2 E_u + 3 \langle A'_i A'^2_o \rangle D_u E_u^2 + \langle A'^3_o \rangle D E_u^3 \qquad (9)$$

Similar approaches lead to formulations for the v- and w-fluctuations from which the Reynolds shear stresses are obtained. For example $\langle u'v' \rangle^+$ follows with:

$$\langle u'v' \rangle^+ = \langle A'_i B'_i \rangle D_u D_v + \langle A'_i B'_o \rangle D_u E_v + \langle A'_o B'_i \rangle E_u D_v + \langle A'_o B'_o \rangle E_u E_v \qquad (10)$$

Here, B_i' and B_o' denote the time-dependent factors of the decomposition for the v-component of the fluctuation. In each equation from (8) to (10) the first term denotes the pure inner contribution and the last term the pure outer contribution. All other terms indicate interactions between inner and outer regions. Figure 3 shows an example for the representation of the streamwise stress in comparison with experimental results (HWA, l^+ <10) and figure 4 shows three distributions of third-order moments in comparison with DNS CH data from Hoyas & Jimenéz (2005). In both cases reasonable good agreements is achieved.

CONCLUSIONS

In this study scaling and modeling of wall-bounded flows are addressed. In the first part, it is demonstrated that classical scaling based on inner variables alone is not applicable for any of the stresses. In all cases with exception of the peak position of the streamwise stress, significant Kármán number dependencies remain. An analysis of the wall values of streamwise skewness and flatness confirms this disadvantage of classical inner scaling for higher-order moments. In extending our previous work, we show that these dependencies can be removed when an alternative mixed scaling is applied. Based on the general finding that throughout the entire wall-layer inner and outer scales are of importance, a model approach for the fluctuations is presented. The agreement of this approach with experiments is shown.

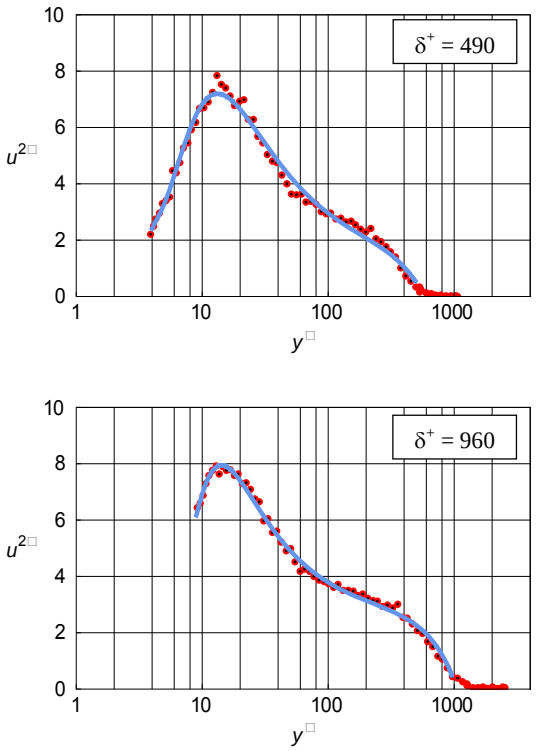

Figure 3: Comparison of streamwise stress experiment (red symbols) and proposed model (blue curves).

[2] As an example, the derivation is done here for the streamwise component.

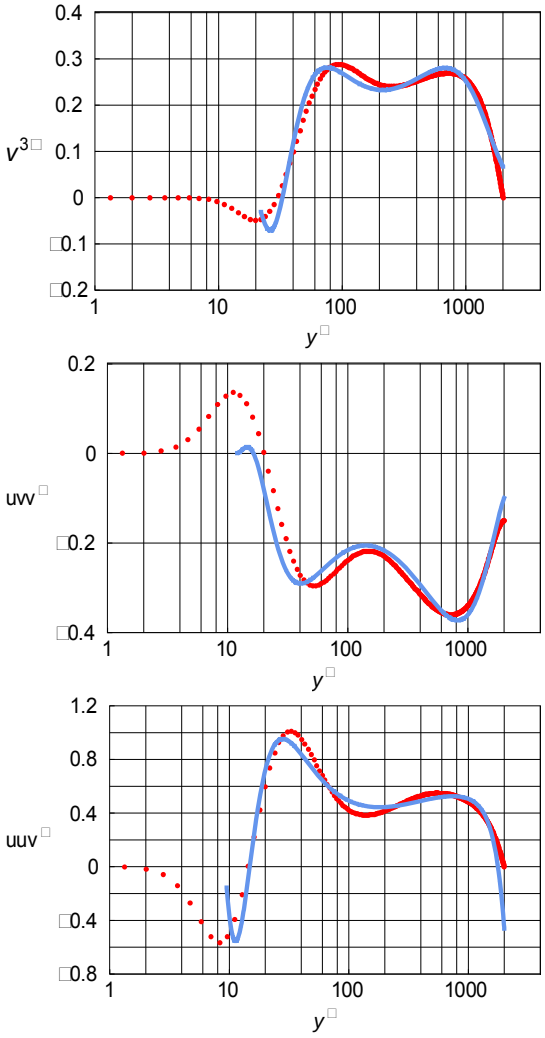

Figure 4: Comparison of higher order moments from DNS realization (red symbols) and proposed model (blue curves). DNS data from Hoyas & Jimenéz (2005) with $Re_\tau = 2004$.

Acknowledgement

We thank L. Keirsbulck, G. Fourrié and L. Labraga from Université de Valenciennes, France, for supporting us with their experimental data for the validation shown in Fig. 3.

REFERENCES

Bruns, J., Dengel, P., and Fernholz, H. H., 1992, "Mean flow and turbulence measurements in an incompressible two-dimensional turbulent boundary layer Part I: data," Hermann-Föttinger Institut für Thermo- und Fluiddynamik, TU-Berlin.

Buschmann, M. H., and Gad-el-Hak, M., 2010, "Normal and cross-flow Reynolds stresses: differences between confined and semi-confined flows," *Exp Fluids*, Vol. 49, pp. 213-223.

Buschmann, M. H., Indinger, T., and Gad-el-Hak, M., 2009, "Near-wall behavior of turbulent wall-bounded flows," *Int J Heat Fluid Flow*, Vol. 30, pp. 993-1006.

DeGraaff, D. B., and Eaton, J. K., 2000, "Reynolds-number scaling of the flat plate turbulent boundary layer," *J Fluid Mech* Vol. 422, pp. 319-346.

Hoyas, S., and Jimenéz, J., 2005, "Scaling of velocity fluctuations in turbulent channels up to $Re_\tau = 2003$," *Center for Turbulence Research Annual Research Briefs* pp. 51–356.

Hu, Z. W., Morfey, C. L., and Sandham N. D., 2006, "Wall pressure and shear stress spectra from direct simulations of channel flow," *AIAA J*, Vol. 44, 1541-1549.

Iwamoto, K., Suzuki, Y., and Kasagi, N., 2002, "Reynolds number effect on wall turbulence: toward effective feedback control," *Int J Heat Fluid Flow*, Vol. 23, pp. 678-689.

Jimenéz, J., Hoyas, S., Simens, M. P., and Mizuno, Y., 2010, "Turbulent boundary layers and channels at moderate Reynolds numbers," *J Fluid Mech*, Vol. 657, pp. 335-360.

Kim, J., Moin, P., and Moser, R., 1987, "Turbulence statistics in a fully developed channel flow at low Reynolds number," *J Fluid Mech*, Vol. 177, pp. 133-166.

Marusic, I., McKeon, B. J., Monkewitz, P. A., Nagib, H. M., Smits, A. J., and Sreenivasan, K. R., 2010, "Wall-bounded turbulent flows at high Reynolds numbers: Recent advances and key issues," *Physics of Fluids*, Vol. 22, 065103.

Mathis, R., Monty, J. P., Hutchins, N., and Marusic, I., 2009, "Comparison of large-scale amplitude modulation in turbulent boundary layers, pipes, and channel flows," *Physics of Fluids*, Vol. 21, 111703.

Monty, J. P., Hutchins, N., Ng, H. C. H., Marusic I., and Chong, M. S., 2009, "A comparison of turbulent pipe, channel and boundary layer flows," *J Fluid Mech*, Vol. 632, pp. 431-442.

Nagano, Y., Tagawa, M., and Tsuji, T., 1992, "Effects on adverse pressure gradient on mean flow and turbulence statistics in a boundary layer," In: Durst, F., Friedrich, R., Launder, B. E., Schmidt, F. W., Schuhmann, U., Whitelaw, J. H. (Eds.), *Turbulent Shear Flow*, Vol. 8. Springer, Berlin, pp. 7-21.

Nieuwstadt, F. T. M., and Bradshaw, P., 1997, "Similarities and differences of turbulent boundary-layer, pipe and channel flow," In Boundary-Layer Separation in Aircraft Aerodynamics, eds. Henkes RAWH & Bakker PG, Delft University Press, Delft, pp. 15-22.

Schlatter, P., Örlü, R., Li, Q., Brethouwer, G., Fransson, J. H. M., Johansson, A. V., Alfredsson, P. H., and Henningson, D. S., 2009, "Turbulent boundary layers up to $Re_\Theta = 2500$ studied through simulation and experiment," *Physics of Fluids*, Vol. 21, 051702.